Thesis Title

Department of Physics, The University of Hong Kong, Pokfulam Road, Hong Kong

Wang Wenchao
3030053350

Contents

Abstract

Recent observations find that some millisecond pulsars (known as Class II MSPs) show aligned pulse profil es in different energy bands. Conventionally, radio and gamma-ray emission are produced in different regions—in polar cap and outer gap respectively. The finding of Class II MSPs implies that radio, X-ray and gamma-ray emission can all be emitted in outer gap. This means that Class II MSPs can have a different emission mechanism. Recently, scientists propose a model suggesting that hard X-ray can be emitted by inverse Compton scattering between radio waves and energetic charged particles. The objective of the thesis is to test this model by measuring hard X-ray spectra of some Class II MSPs using *NuSTAR*.

Chapter 1

Introduction

1.1 Neutron Stars and Pulsars

Neutron stars are produced by a supernova explosion of massive stars which have about 4 to 8 solar mass. After the supernova explosion, the star leaves a central region. And the central region collapses because of the effect of gravity until protons and electrons combine to form neutrons ($e^- + p \rightarrow n + \nu_e$) —the reason why they are called "neutron stars". Because neutrons have no electromagnetic force on each other, they can be squeezed very tightly. Therefore, a neutron star has tremendous high density (about $5 \times 10^{17} kg/m^3$) and its diameter and mass is about 20km and 1.4 solar mass respectively. What prevents a neutron star to continue to contract is the degeneracy pressure of neutrons.

Pulsars are fast-spinning neutron stars. Their rotational periods can be from a few milliseconds to several seconds. For example, the rotational period of PSR B1937+21 is about $1.56ms$ while PSR B1919+21 is approximately $1.34s$. As we know, a star can be ripped by centrifugal force if the star rotates too fast. We can estimate lower limit of density of a star with the equation: $\rho = \frac{3\pi}{P^2 G}$, where P is the rotational period of a pulsar. Just for simplicity, we let P be $1s$. Then we get $\rho \approx 1.4 \times 10^{11} kg/m^3$. With the knowledge that the density of a white dwarf is about $1 \times 10^9 kg/m^3$ which is smaller than the lower density limit, the observed fast-spinning stars belong to the kind of stars which are much denser than white dwarf. As a result, neutron stars are ideal candidates for pulsars.

More than 2000 pulsars have been found so far. Most of them are in the disk of our Galaxy while we also can find a small portion of them in high latitude, which can be seen clearly in the figure 1.1. This may because they cannot escape the gravitational potential if their kinetic energy is not large enough. Besides, even though they have large enough velocities to escape from their birth region, there are some probabilities that they become nearly non-detectable before reaching high latitude.

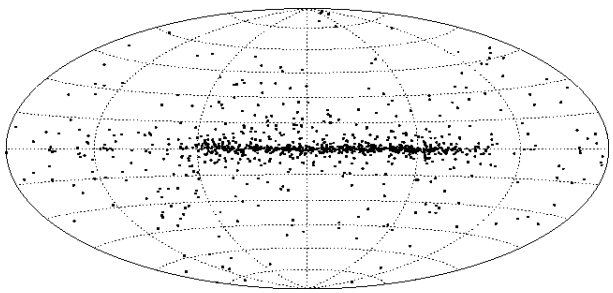

Figure 1.1: *Spatial distribution of some pulsars in galactic coordinate system.*

1.2 Emission Mechanism of Pulsars

Although emission mechanism of pulsars has not been fully understood yet, some models are developed trying to explain observational facts. The following is one toy model that can explain some basic features of pulsars.

1.2.1 Magnetic Dipole Model

Assume a pulsar has a magnetic dipole moment $\vec{m}$, the angel between rotation axis and direction of $\vec{m}$ is α, its angular velocity is Ω, radius is R and moment of inertia is I. Also by assuming that energy of electromagnetic radiation are all from rotational energy, its spin-down rate can be written as:

$$\dot{\Omega} = -\frac{B_p^2 R^6 \Omega^3 \sin\alpha^3}{6c^3 I}$$

where B_p is magnetic field strength in the pole of the pulsar. Its surface magnetic field can also be estimated by:

$$B_s = \sqrt{\frac{3c^3 I}{2\pi^2 R^6} P\dot{P}} = 3.2 \times 10^{19}\sqrt{P\dot{P}}$$

where B_s is the strength of surface magnetic field.

In general, a pulsar's spin down rate can be expressed as: $\dot{\Omega} = -K\Omega^n$, where K is a constant and n is called braking index. In magnetic dipole model n is 3 (*H.Tong 2015*). Then characteristic age of the pulsar can be defined as: $P/2\dot{P}$ in magnetic dipole model. For example, the Crab pulsar's rotation period is about $0.033s$ and period derivative is $4.22 \times 10^{-13} s/s$. The characteristic age is about 1200 years. The pulsar is remnant of a supernova which is observed by ancient astronomers in 1054 AD, so the record shows that characteristic age can give us order of magnetic estimate of a pulsar's real age.

Although braking index is 3 in magnetic dipole model, most of pulsars' braking index is less than 3 as shown in figure 1.2. The reason is that if a pulsar's spin down is completely because of pulsar wind, the braking index is 1. Thus, the real braking index should be a combination of 1 and 3, which is usually less than 3 (*Oliver Hamil 2014*).

Pulsar	n_{obs}	Ω	$\dot{\Omega}$
		s^{-1}	$10^{-10} s^{-2}$
PSR B0531+21 (Crab)	2.51±0.01	30.22543701	-3.862283
PSR B0540−69	2.14±0.01	19.8344965	-1.88383
PSR B0833−45 (Vela)	1.4±0.2	11.2	-0.157
PSR B1509−58	2.839±0.001	6.633598804	-0.675801754
PSR J1846−0258	2.16±0.13	3.0621185502	-0.6664350
PSR J1833−1034	1.857±0.001	16.159357	-0.5275017
PSR J1119−6127	2.684±0.001	2.4512027814	0.2415507
PSR J1734−3333	0.9±0.2	0.855182765	-0.0166702

Figure 1.2: *Braking index of some pulsars.*

1.2.2 A More Sophisticated Model

It is oversimplified to regard a pulsar as a magnetized sphere rotating in vacuum. Actually, there are plenty of charged particles in a pulsar's magnetosphere which corotate with the pulsar. The creation

of charged particles can be described by the following steps (*P.A.Sturrock 1971*).

1. The corotating charged primary particles emit gamma-ray by curvature radiation because of acceleration in super strong magnetic field.

2. In super intense magnetic field, the high energy photons decay into electrons and positrons which are called secondary particles by the process: $\gamma + (B) \rightarrow e^+ + e^- + (B)$. Syncrotron photons can be emitted by these secondary particles.

3. Secondary particles are also accelerated in strong magnetic field which is just like primary particles. As a result, these charged particles can create more secondary particles.

This chain of process is quite efficient to produce charged particles and pulsar's magnetosphere is filled with plasam as a consequence. So, it is natural to think of the distribution of charges in pulsar's magnetosphere. A characteristic charge density $\rho_{GJ} = -\frac{\vec{\Omega}\cdot\vec{B}}{2\pi c}$ is called Goldreich-Julian density. This charges can offset part of electric field ($E_\parallel$) which is parallel to magnetic field. There is some region in the magnetosphere called "outer gap" where ρ_{GJ} is so small that it can't screen $E_\parallel$ effectively. As a result, the secondary particles can be accelerated at a very large velocity (Lorentz factor $\gamma \sim 10^7$) and emit gamma-ray. Photons in outer gap can also create electrons and positrons by the process: $\gamma + \gamma \rightarrow e^- + e^+$. At the outer gap, one-photon pair production can't happen because magnetic field is too weak in this region.

1.3 Millisecond Pulsar

1.3.1 P-$\dot{\text{P}}$ Diagram

P-$\dot{\text{P}}$ diagram is an important tool for analyzing evolution of pulsars. Period (P) and time derivative of period ($\dot{\text{P}}$) are two of pulsars' important characteristics. Analyzing the position of a pulsar in P-$\dot{\text{P}}$ diagram can give some valuable information such as which evolution stage the pulsar is in or the type of the pulsar, etc. The figure 1.3 is an example of P-$\dot{\text{P}}$ diagram. The horizontal axis is pulsars' rotation periods and the vertical axis is time derivative of rotation periods. In this P-$\dot{\text{P}}$ diagram,

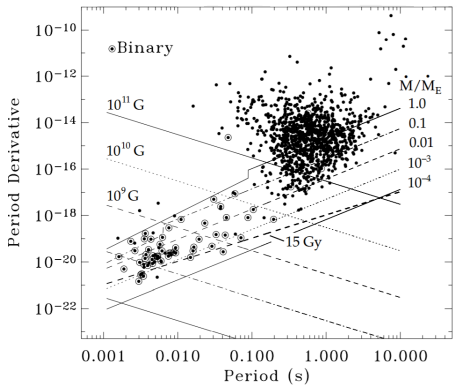

Figure 1.3: *Position of pulsars in P-$\dot{P}$ diagram*

the negative slope lines represent the strength of surface magnetic field while the positive slope lines represent the characteristic age of pulsars. The following is a short explanation for this. From previous discussion, we have known that the characteristic age of a pulsar is $\tau = -P/\dot{P} = P/(-\dot{P})$, so line of constant τ is a set of straight lines with equal positive slope. We also know $B \propto \sqrt{P\dot{P}}$, therefore the line of constant B should be a part of hyperbola. When $\dot{P}$ is very small, the hyperbola looks like a straight line with negative slope.

This figure shows that most pulsars lie in the position about $1s, 10^{-14}s/s$. At the same time, a couple of stars lie at the bottom-left of the figure—these are millisecond pulsars (MSP). Their rotation periods are about 1-20 milliseconds. It is believed that MSPs are spun up by accretion of mass from its companion star. In the above P-$\dot{\text{P}}$ diagram, we can observe that millisecond pulsars'

surface magnetic field are about 3 to 4 orders of magnitude lower than those of normal pulsars. However, an MSP has a relative strong magnetic field near its light cylinder. The reason is that an MSP's radius of light cylinder ($R_{lc} = c/\omega$) is much smaller than a normal pulsar's because of its short rotation period and the magnetic field near light cylinder can be estimated as $B_{lc} \sim (R/R_{lc})^3$. At the same time, pulsars' emission mechanism is closely related to their magnetic field near light cylinder. As a result, like a normal pulsar, an MSP also have broadband spectrum from radio to gamma rays.

1.3.2 Origin Of Millisecond Pulsars

From pulsars' emission mechanism, we know that magnetic field of a pulsar decreases with time while the spin period increase with time. But MSPs' spin period is much shorter than normal pulsars and surface magnetic field is a lot weaker. This makes an MSP seem to be both young and old. As a result, people think millisecond pulsars are old pulsars spun up by its companion. The companion star transfer mass and angular momentum to accelerate the pulsar. Therefore, the aged pulsar can spin faster gradually.

Mass Transfer And Accretion In Binary Systems

X-ray binaries are a type of binary systems that is luminous in X-ray band. There are several kinds of X-ray binaries including low mass X-ray binaries (LMXB) and high mass X-ray binaries (HMXB). The way of transferring mass is different in these two types of systems. Before discussing mass transfer, we need to know a little bit about Roche Lobe. The figure 1.4 is a schematic diagram of Roche lobe.

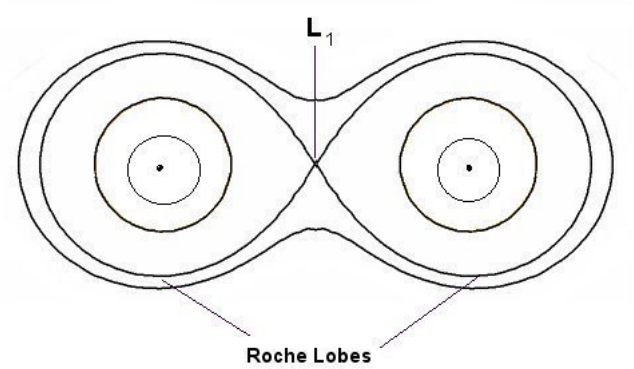

Figure 1.4: *Schematic diagram of Roche lobe.* L_1 is called inner Lagrange point which is the intersection of equipotential lines of star A and B.

We call two stars in an LMXB as A and B respectively for convenience. It is obvious that if an object is close to star A, the gravitational influence of A is so strong that we can nearly ignore the effect of star B. Similarly, this is true for star B. As a result, there must be a point where the effect of star A is equal to star B which is called inner Lagrange point (*Seidov 2013*). The two volumes inside the largest equipotential lines of A and B are called Roche lobe. If star B cross its Roche lobe, than its mass will be attracted by A thus mass transfer between A and B happens. We should notice that this is the main way of mass transfer in LMXB. While in HMXB, the mass can be transferred by strong wind of the massive companion star.

What should be noted is that mass transfer can change the distance between two companion stars. If low-mass star transfer mass to high-mass companion star, the orbital separation will be large. This can actually stop mass transfer and is like negative feedback. On the contrary, mass transfer from high-mass star to low-mass star will shrink the orbital distance.

1.3.3 Class II MSPs

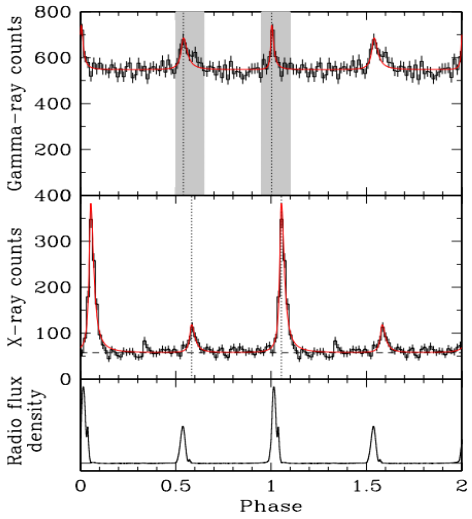

Figure 1.5: *Pulse profiles of PSR B1937+21 in radio, X-ray and gamma-ray.*

Radio emission are usually considered to be emitted above the polar cap, which means radio emission and gamma-ray emission are from different location of pulsar's magnetosphere. However, there are about 10 sources showing aligned pulse profiles in radio and gamma-ray implying that radio emission may produced from outer magnetosphere and they are called Class II MSPs (*Guillemot et al. 2012*). These pulsars have strong magnetic field near the light cylinder. The figure 1.5 is an example of aligned pulse profile.

1.4 Objectives

Recently, it is found that X-ray band of spectrum of millisecond pulsar B1937+21 has a hard photon index of 0.9±0.1 by analysing data of *Chandra*, *XMM-Newton Fermi* (*Ng et al. 2014*). People think X-ray emission is mainly produced by synchrotron radiation, but it is difficult to explain such a hard photon index. Besides millisecond pulsar B1937+21, it is discovered that hard photon index is a common characteristic of class II MSPs. Therefore, people propose that Inverse Compton scattering can also lead to X-ray emission and build a model recently to explain it (*Ng et al. 2014*).

In order to test the model, we need to analyse the hard X-ray band of millisecond pulsars B1937+21, J0218+4232 and B1821-24. The energy ranges of *Chandra* and *XMM-Newton* are up to 10keV and 15keV respectively while *NuSTAR* can be up to 79keV. As a result, we aim to use *NuSTAR* to measure the hard X-ray band of the three MSPs mentioned above.

1.5 NuSTAR

NuSTAR stands for Nuclear Spectroscopic Telescope Array and is launched in June 12, 2012. It is the first space telescope focusing on hard X-ray (3eV-79eV) band. This is the telescope that we mainly use and it is helpful to know the structure to deal with its data. It mainly composed of three parts: detectors, optics and mast as the figure 1.6 shows.

1.5.1 Detectors

NuSTAR has two independent photons counting detector modules (FPMA & FPMB) and each module contains 4 Cadmium-Zinc-Telluride (CZT) detectors. Every detector is a rectangular crystal

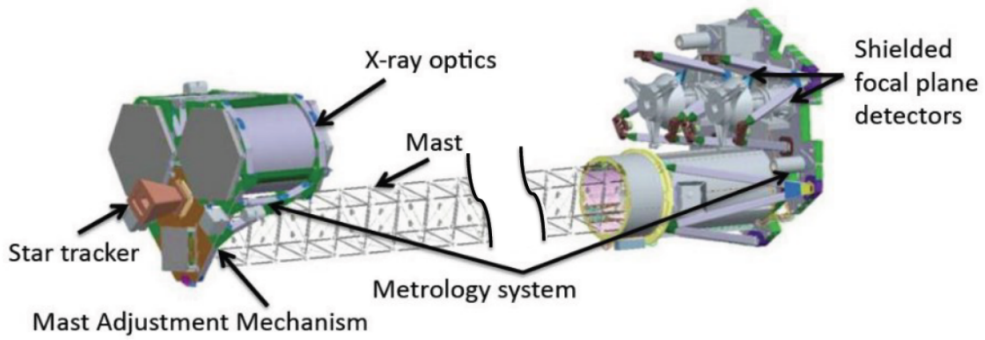

Figure 1.6: *NuSTAR's sketch. The mast connects X-ray optics and focal plane detectors.*

whose size is $20mm \times 20mm \times 2mm$ (length$\times$ width$\times$height) and have 32×32 pixels.

In order to help to distinguish the source photons and the background photons, the focal planes

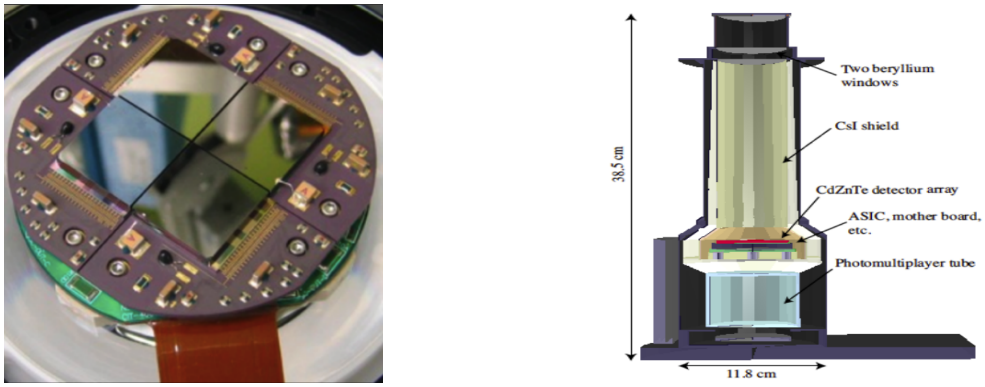

Figure 1.7: *Left: One of two detector modules which contains 2×2 array of independent detectors. Right: One detector module shielded by Csl crystal. CZT detectors can turn high energy photons into electrons very efficiently in room temperature so they are operated at 15°C.*

are shielded with crystals made of Celsium-Iodide (Csl). The Csl shields can record the photons come from directions which are not the direction of *NuSTAR* optical axis. So background photons can be subtracted from the total photon counts.

1.5.2 Optics

Corresponding to two detector modules, *NuSTAR* also has two optics called Optics Module A and B (OMA & OMB). The focal length is 10.14 meters which is about the same length with its mast. X-ray is very hard to reflect so mirrors are usually made of high density materials such as Pt and W. Past telescopes such as *Chandra* uses these high density materials to reflect low energy X-ray (up to 10eV). However, the efficiency of reflecting high energy X-ray drops drastically. High density contrast between two kinds of materials are needed to overcome this problem. As a result, *NuSTAR*'s mirror is coated with Pt/SiC and W/Si multilayers and can reflect hard X-ray up to 79eV.

Besides high density contrast between two materials, a small incident angle is also required. As the figure 1.8 showing, the focal length may be very long because of the small incidence angle. This is partly the reason why *NuSTAR*'s detectors and optics are separated by a 10-meter long mast which will be introduced in the next section.

1.5.3 Mast

Although *NuSTAR*'s mast is stable and reliable, it can cause some image distortion because of its deformation. Therefore, careful calibration or measurement of mast's deformation is necessary. In

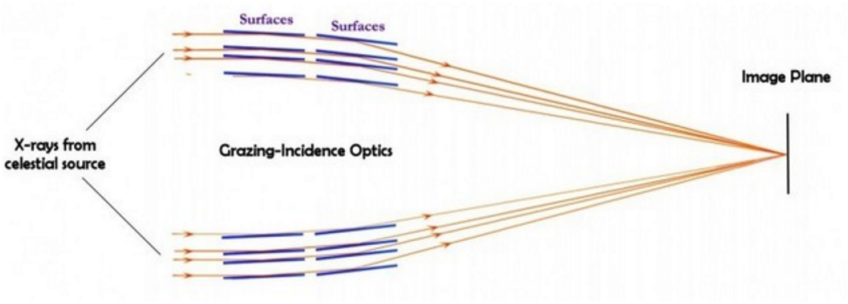

Figure 1.8: *Light path schematic diagram of reflecting X-ray*

order to achieve this, *NuSTAR* has a laser metrology system which consists of two lasers and two light-sensing detectors. The two lasers are located on optics while the two detectors are mounted on the detector module. Then, the deformation can be recorded and used to reconstruct the raw data. The figure 1.9 shows what the mast looks like. The reason why *NuSTAR* has a deployable mast is that it is carried by a relative small rockets.

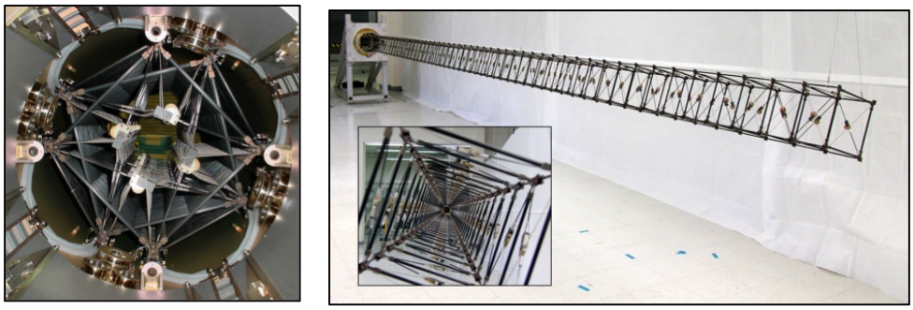

Figure 1.9: *NuSTAR's mast. Left: stored in container. Right: after being deployed.*

1.5.4 Performance of NuSTAR

Though *NuSTAR* has a broad energy range, the effective collecting area at different energy is quite different. The figure 1.10 shows comparison between *NuSTAR* and other telescopes.

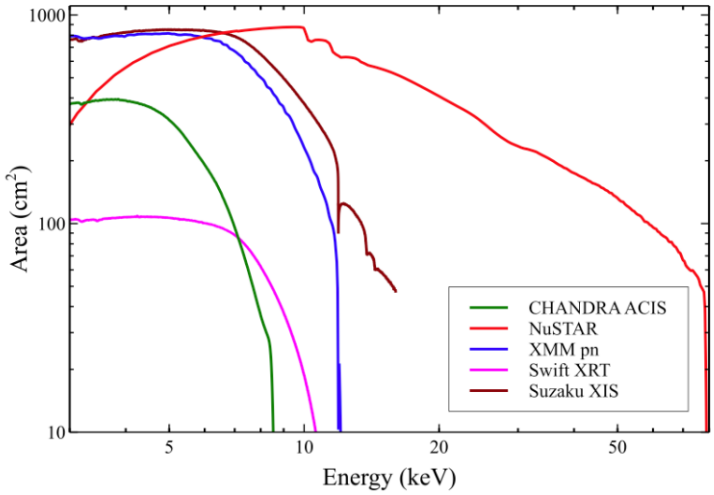

Figure 1.10: *NuSTAR's effective area compared with other X-ray focusing telescopes.*

From figure 1.10 we can see that the effective area drops dramatically after 70keV. Therefore, we may need to screen out the high energy part (>70keV) for data analysis. The figure 1.11 shows

the point spread function (PSF) of optics module A and B. In order to make faint pixels look more obvious, the images are in logarithm scale. The PSF of both optics module A and B are dependent on energy. The table 1.12 lists the relationships and from this table we can also see that angular resolution of optics module B is slightly better A.

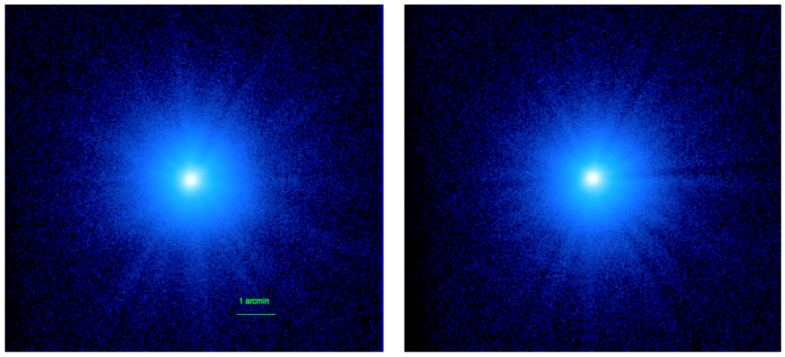

Figure 1.11: *Image of NuSTAR's point spread function of optics module A(left) and B(right).*

Energy (keV)	FPMA HPD (″)	FPMB HPD (″)
3 – 4.5	70.3	65.6
4.5 – 6	67.1	62.6
6 – 8	64.7	60.7
8 – 12	63.5	59.5
12 – 20	63.4	60.3
20 – 79	63.4	62.4

Figure 1.12: *PSF (half power diameter) as a function of energy.*

1.6 The Procedures of Processing NuSTAR Data

NuSTAR Data Analysis Software (*NuSTARDAS*) is used for data processing. This includes three steps: data calibration, data screening and products extraction. The next paragraph talks about the reason the first two steps are necessary.

Lots of factors can affect raw data, such as movements of *NuSTAR*'s mast, the orbit of the telescope, etc. As a result, *NuSTAR* data must be calibrated before they can be used to do data analysis. Also, some parts of data are not good for scientific analysing. For example, there are some bad pixels in the telescope's detectors which cannot record photons correctly. Thus, the data recorded by these bad pixels have to be treated very carefully. We might get rid of the data when the source is bright, while if the photon counts are too small, we might have to use these data with carefulness. And sometimes we may want to focus on a particular part of data. Thus, we need to screen the calibrated data.

In order to understand data filter process better, it is necessary to know the different levels of *NuSTAR* data. *NuSTAR* data can be divide into 5 levels which is from level 0 to level 3. Level 0 data are raw telemetry files which might not be in formal format (FITS format). Level 1 data contains two parts: level 1 and level 1a. Level 1 data are formatted in FITS format, but not calibrated yet. Level 1a data are level 1 data after calibration. Actually, level 1a data are addition of level 1 data and calibration data. Level 1a data are produced by step 1 (data calibration). Then by step 2 (data screening), we get level 2 data which are cleaned files. We can do data analysis after getting level 2

data. Thus in order to get reliable result, it is key to get raw data properly cleaned. The figure 1.13 is comparison between level 1a event file and level 2 event file after screening.

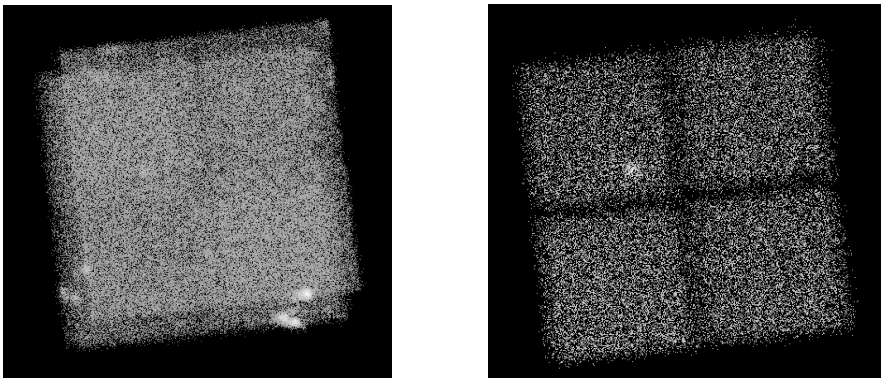

Figure 1.13: *Left: sky image generated directly from level 1a data. Right: sky image generated from screened level 2 data. These two figures are produced from the same raw data. There are many criteria for data screening and the figure in the right is just an example.*

1.6.1 Data Calibration

The first process is data calibration. In this step, two factors should be considered: the temporal change of mast and spacecraft's attitude. By using telescope's housekeeping files, the corrected data can be produced by *NuSTAR* software. There are some *NuSTAR* software modules for this process. Most of them are nearly automatically, which means once we have initial files, the output files are fixed. Therefore, we do not concentrate much on these software modules. Before we go into this module, some basic concepts should be introduced.

Grade of Data

When a photon interacts with a detector, the ideal condition is that only one pixel record this photon, which has better spectra resolution than other situations. But a single X-ray photon can be spread and received by more than one pixel. Generally, the less pixels by which a photon recorded, the better the event is. Naturally, there are different patterns of interaction between the photon and surrounding pixels. These patterns are listed in figure 1.14.

Status of Data

Just like flagging the quality of pixel data, it is necessary to flag event data because there are many factors that can trigger detectors. For instance, if we have a photon record in a detector, we need to know if it is from the source we are observing. Actually, cosmic rays can also trigger the detectors and we want to get rid of them in order to increase the signal to noise ratio. Therefore, after we have distinguished them from source photons, it is needed to be recorded for data screening—thus each single event has its status. In fact, similar to data's grade, status of data also has many patterns. For example, an event may fall into bad pixels, have a neighborhood bad pixel or fall into a hot pixel, etc. All these different situations are recorded by a 16-bit binary number and status of good event which is ideal for scientific analysis is all zero (recorded as "b0000000000000000").

1.6.2 Data Screening

After data calibration, though we know if one event is good or not, bad events are not excluded from original files. This is the primary reason of doing data screening. There are primarily 3 procedures

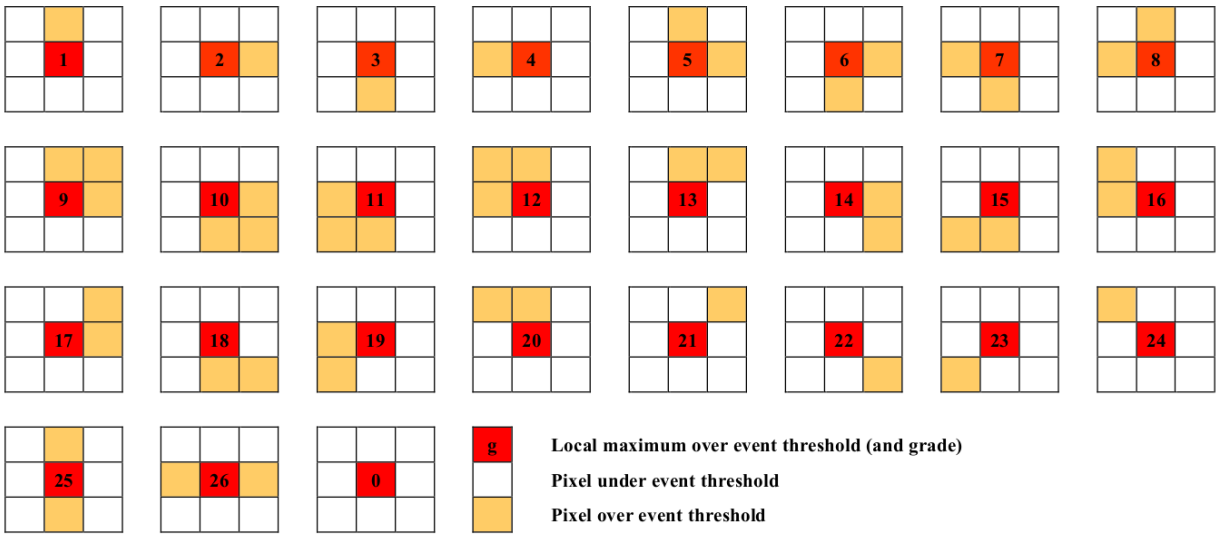

Figure 1.14: *There are 33 different NuSTAR grades—from grade 0 to 32. In this figure, grades from 0 to 26 are listed because these grades are accepted by NuSTAR data screening by default. We can further get rid of some grades if needed.*

in this step.

The first one is choosing good time intervals, which means remove some unwanted time intervals. For example, when the telescope is in the South Atlantic Anomaly, when the Earth is in the Field Of View and when the motion of mast is not well tracked, etc. Sometimes we need to add our own GTI (Good Time Interval) file to get better cleaned data. Then remove bad pixels and events flagged as bad in the last step (by using the information of data status). At last, choose the proper grade of data (the default value is 0-26).

The core module in this step is called 'nuscreen' and most of job is done by this software module. There are two parameters we mostly focus on—'gradeexpr' and 'statusexpr', which are used for choosing grade of data and status of data respectively. For example, gradeexpr=0-8 means choosing grade range from 0 to 8 and statusexpr="STATUS==b000000000x0xx000" means leaving out bad events. We also can set them to default value by 'statusexpr=DEFAULT' and 'statusexpr=DEFAULT'. By adjusting these parameters' values, we can get a bunch of cleaned event files. Then we can generate several sky images and spectra and choose a better result.

1.6.3 Products Extraction

The aim of this process is to extract high-level scientific products including light curves, sky images, spectra, Ancillary Response Files (ARF) and Redistribution Matrix Files (RMF). ARF and RMF files are used for spectra analysis. The main software module is 'nuproducts' which generates these files automatically by passing some parameters. I mainly focus on two parameters which are 'pilow' and 'pihigh'. These two parameters filter the energy range of cleaned stage 2 event files. The default values of the two parameters are 39 Pi and 1909 Pi respectively corresponding the *NuSTAR*'s energy range 3-78.4eV. But usually we choose pilow larger than 39 and pihigh smaller than 1909 in order to get more reliable data.

Chapter 2

Data Analysis

2.1 Data Analysis of Pulsar B1937+21 Using NuSTAR

Usually, we choose all the parameters to be default values. We may change some of the parameters in certain cases. Then we can produce a complete set of stage 2 files by using the module 'nupipeline'. The following is the sky images from *NuSTAR*'s module A and module B.

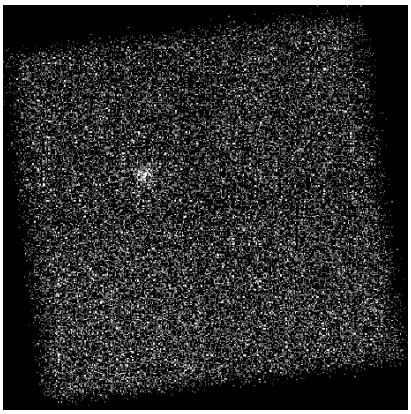

Figure 2.1: *Sky image of module A*

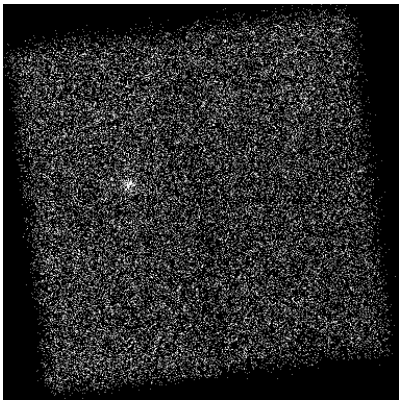

Figure 2.2: *Sky image of module B*

Although there are lots of background noises in these two pictures, the source is clearly identifiable. We can obviously see the differences between these two figures. For example, the source is sharper in the right figure. Actually, from figure 1.12 we can see that the PSF (half power diameter) of module B is slightly smaller than that of module A in each energy range. The focal plane module comprises 4 detectors, but in these figures we can barely distinguish different detectors. This implies that the data are not calibrated and screened well enough.

After getting cleaned stage 2 files, we can continue to generate light curves, spectra and so on. Before doing these, it is required to choose source and background regions. The figure 2.3 show the regions we choose.

In figure 2.3, the left green circle is source region while the right green circle is background region. The center of source circle is (19:39:38.561 ra, +21:34:59.126 dec) and the radius is 23 arcseconds. The center of the background region is (19:39:12:412 ra, +21:35:29.210 dec) and the radius is 34.140 arcseconds. We call the choice of the source and background region as "region 1". The data of the source region center is from *ATNF* (Australia Telescope National Facility). From the figure 2.3 we can see that the source we observed is actually the right source—B1937+21. This means that the observation data can be used to analyse the pulsar B1937+21. However, for module B, the position observed source is a little bit away from the ATNF data. This means that we might need 2 sets of source and background regions for module A and module B respectively.

The figures 2.4 and 2.5 are the light curves of module A and B. These light curves are generated

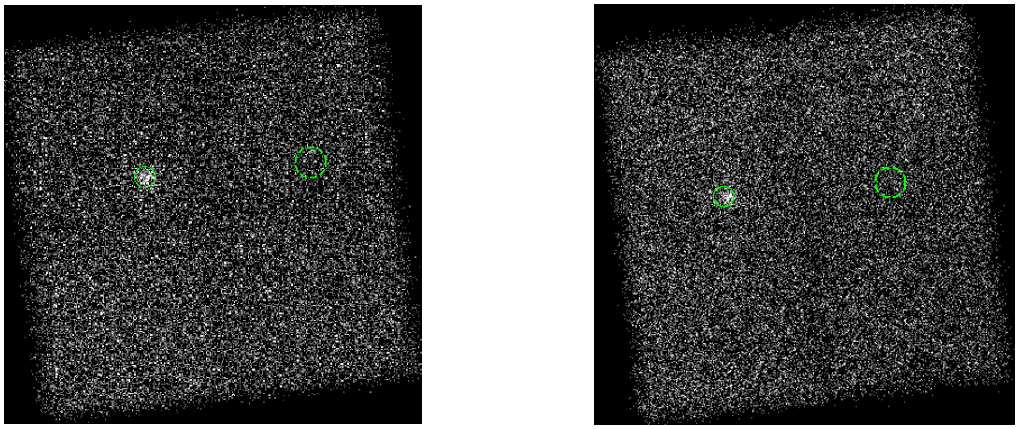

Figure 2.3: *Source and background regions of module A (left) and B (right).*

using ds9 software. The time interval of each bin is 50 seconds. The horizontal axis is time and the vertical axis is proportional to count rate. Although these pictures show periodicities, it does not mean that we can do timing analysis for B1937+21 by using *NuSTAR*. The reason is that the time resolution of *NuSTAR* is about 2 *ms* which is larger than the spin period of B1937+21 (∼1.56ms). In fact, I think the periodicity reflect the *NuSTAR*'s orbital information to some extent. *NuSTAR*'s orbit is very low (the semi major axis is about 7000km) so its observation will be greatly influenced by the Earth. When the source is blocked by the Earth, the count rate is zero (after data calibration and screen).

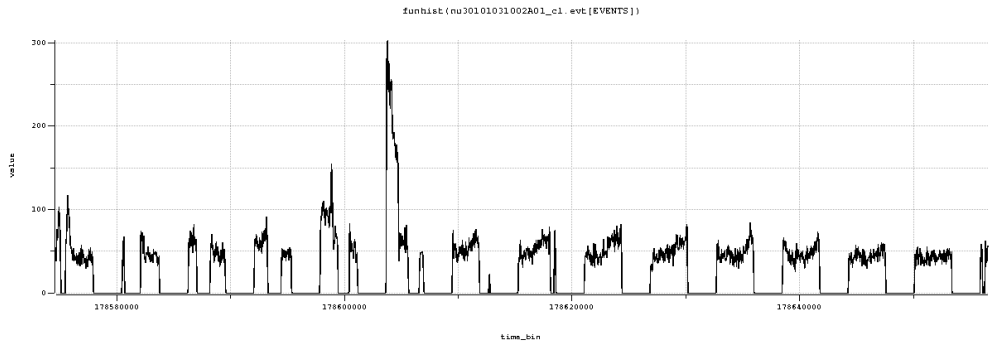

Figure 2.4: *Light curve of module A*

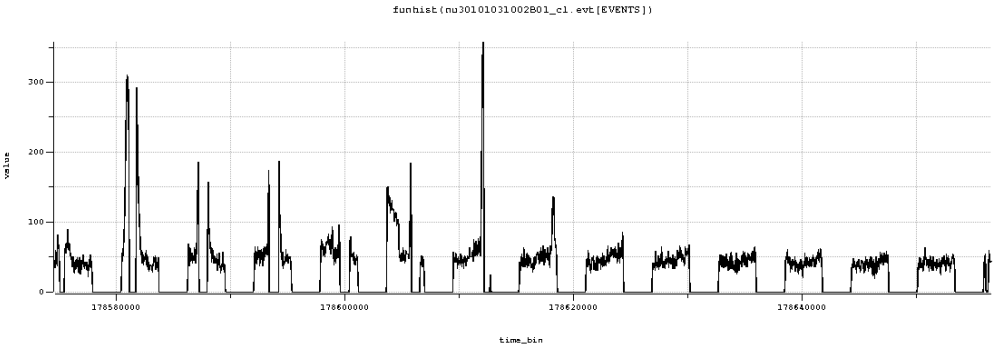

Figure 2.5: *Light curve of module B*

The figure 2.6 is the spectra of module A and B. The group counts of both module A and B are 20 and the fitting model is multiplication of absorption of X-ray model (see in sherpa document 'xstbabs') and 1 dimensional power law model (see also in sherpa document'powlaw1d'). We use chi

square statistics to analyse goodness of fitting.

	Module A	Module B
Column Density (nH) ($10^{22} atoms/cm^2$)	4.06	0.012
Photon Index (Γ)	1.33	1.46
Reduced Chi Square Statistic	0.33	0.30

Table 2.1: *Fitting result*

The table 2.1 lists some important parameters of the fitting result. The number of total points in spectrum of module A and B are both 11. For the spectrum of A, the reduced statistic is about 0.33 and Q-value is about 0.95. The fitted column density is about $4.06 \times 10^{22} atoms/cm^2$ and the photon index is 1.33. For the spectrum of B, the reduced statistic is 0.30 and Q-value is about 0.97. The column density is about 0.012 and photon index is 1.46. We observed that the column density difference between module A and B are huge (module A is about 400 times larger than module B). This is because that the high energy X-ray photons are nearly not absorbed by interstellar medium. As a result, the column density fitted only by *NuSTAR* (3∼79eV) reliable so we need to combine *NuSTAR* data and *Chandra* and *XMM-Newton* data together to fit.

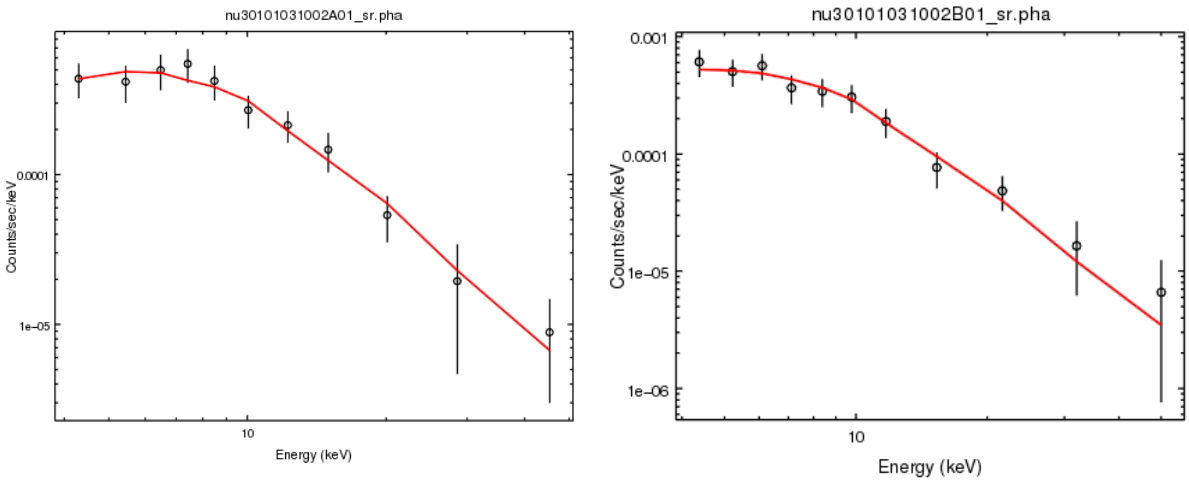

Figure 2.6: *Spectra of module A (left) and B (right). The total source counts of A before grouping is 301 and B is 286. After subtracting background, the source counts of A is 193.45 and B is 170.25. Reduced chi square statistic: 0.33 (A) and 0.3 (B).*

Some Analysis

There are actually some problems in the whole precess. First of all, the regions is not properly chosen. Although we can see that the pulsar is completely in the source region, it is not in the center of the source region (especially for module B). As for the background region, it is a little bit small. In addition, there are four detectors so it is better to choose the background and source region in the same detector.

Secondly, there are many spikes in light curves of both module A and B. Therefore we may need

to clean the data more carefully. One straightforward way is to add our own GTI file rather than only using the default GTI file. Thirdly, the reduced statistic values for module A and B are 0.33 and 0.30 respectively, which are a little bit small. It means that our model is overfitted and the result seems to be too good to happen. In general, our model is good if reduced chi square statistic is about 1. Thus, we need to rethink how we should screen the data.

In short, we are focusing on the two things: change the source and background regions and filter the light curves by adding our own GTI file.

At first, we need to change the source and background regions. The figure 2.7 shows the region we choose this time. There are three major changes of the chosen regions. First of all, we slightly adjust the center of the source region in order to make the observed source be the center of the source region. The center is (19:39:38.101 ra, +24:34:56.838 dec). We do not change the radius of the source region so the radius is still 23 arcseconds. Secondly, we change the position of the background region and make it in the same region with the observed source. The center of the background region is (19:39:38.003 ra, +21:34:57.657 dec). The inner and outer radius (the background region is an annulus) are 40 arcseconds and 100 arcseconds respectively. The reason we choose the background region is that *NuSTAR* has 4 detectors and we want to get rid of the influence of instinct differences between the 4 detectors. Thirdly, we change the shape of background region from a circle to an annulus. Just as before, we call this choice of region as "region 2". The aim is to make the background region surround the observed source to be more like the background of the source.

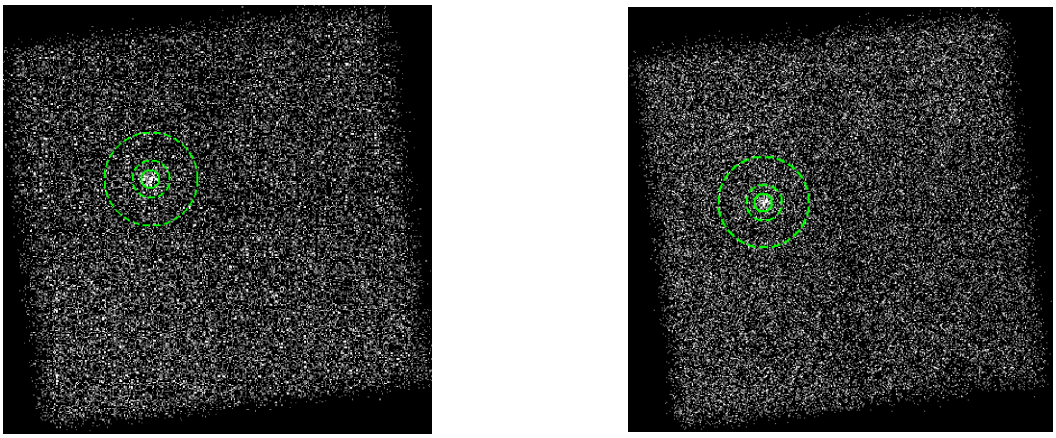

Figure 2.7: *Source and background regions of module A (left) and module B (right).*

At first glance, it seems that this time we choose the source and background region reasonably. But there are also some problems just as the following figure 2.8 showing. The *NuSTAR* is composed of 4 separate detectors that work independently with each other. Therefore, we should make sure that the background region we choose does not cross the border of one detector. Thus, we change the background region to the "region 3" as the right part of the following figures show (figure 2.8) and keep on using the "region 3" in the following discussion of this section. Meanwhile, because we want to try to do timing analysis, barycenter correction is also applied in the following analysis. So far, we have changed 2 things: background region and barycenter correction.

The figures 2.9 and 2.10 are the light curves of the module A and B respectively after changing the source and background regions. The bin time is also 50 seconds. The horizontal axis represents time and the vertical axis represents count rates. Actually there is no obvious improvement in light curves after we change the source and background regions — there are also some spikes in the light curves. In order to get rid of those high spikes, we add some GTI files to filter the event file.

The figure 2.11 is the spectra of module A and B. The table 2.2 show some key parameters of fitting result. The fit model and method are the same as before. For module A, the reduced chi square statistic value is about 0.73 and Q-value is 0.65. For module B, the reduced chi square statistic

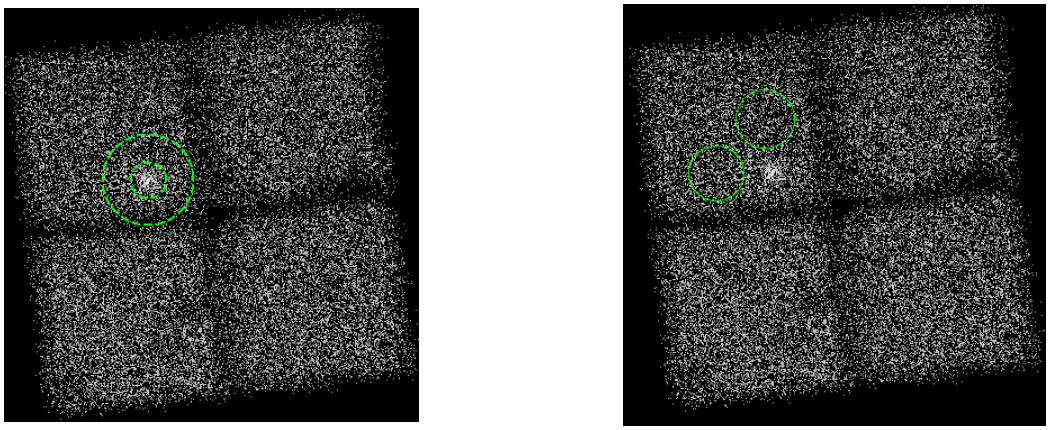

Figure 2.8: *The problems of the annulus background region (denote as "region 2", left) and the background region we choose again (denote as "region 3", right).*

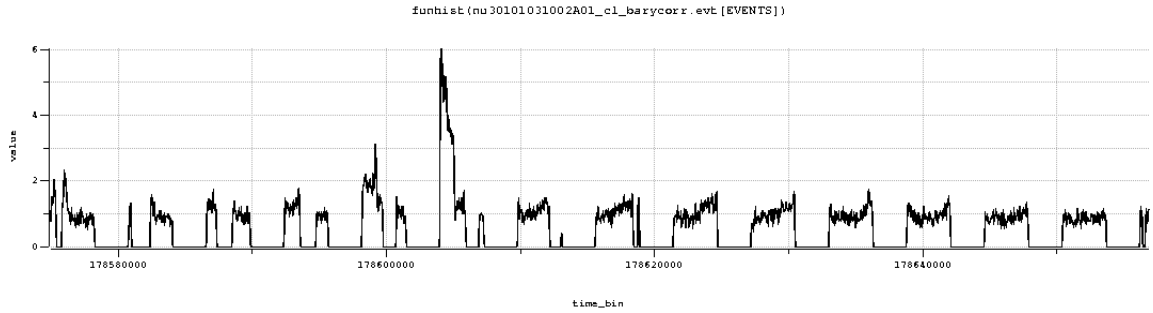

Figure 2.9: *Light curve of module A*

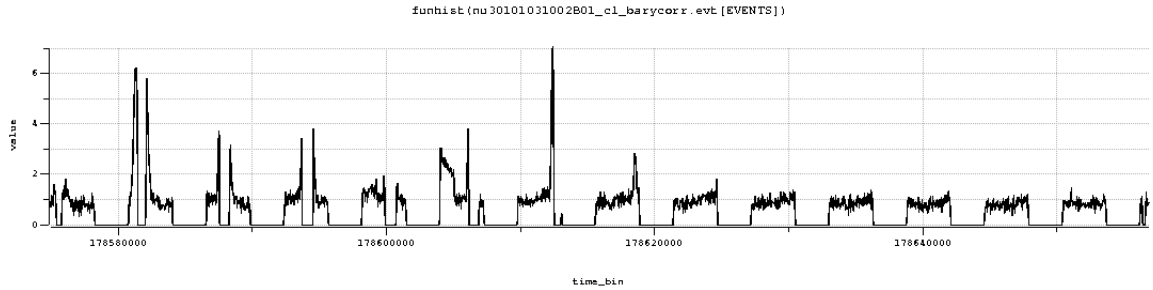

Figure 2.10: *Light curve of module B*

	Module A	Module B
Column Density (nH) $(10^{22} atoms/cm^2)$	6.46×10^{-6}	1.75×10^{-5}
Photon Index (Γ)	1.10	1.53
Reduced Chi Square Statistic	0.74	0.53

Table 2.2: *Fitting result*

is about 0.51 and Q-value is 0.83. After changing the source and background regions, the reduced chi square statistic values of both module A and B are greatly increased while the Q-values are largely decreased. This means that the observation data is less overfitted by our model, which generally is a better result.

Now we consider using our own GTI file to filter the light curves we get before in order to get rid of spikes. We use "dmextract" and "deflare" tools to extract GTI files. The figures 2.12 and 2.13 are the light curves after filtering event files by our own GTI files.

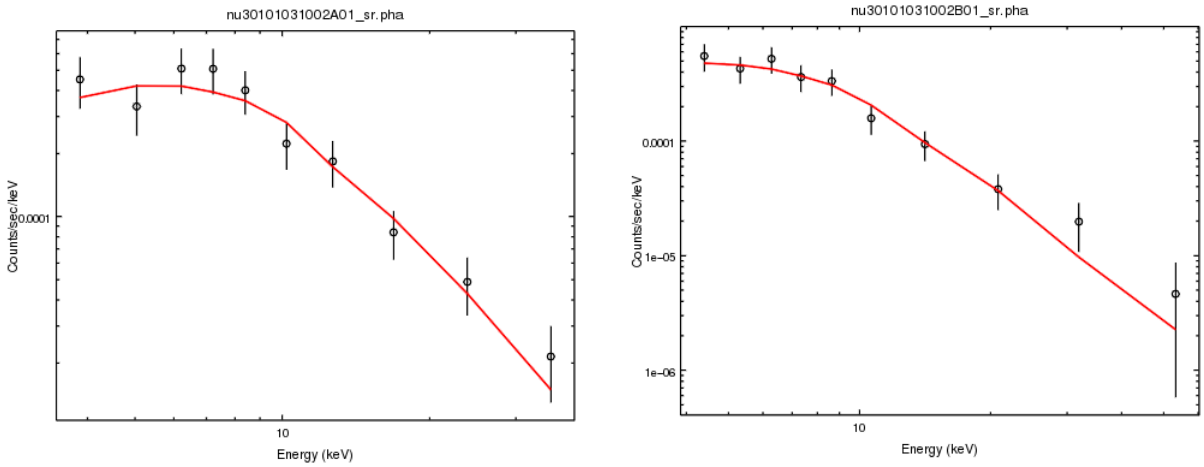

Figure 2.11: *Spectra of module A (left) and B (right). The total source counts of A before grouping is 264 and B is 254. After subtracting the background counts, the source counts are 188.23 (A) and 161.97 (B). Reduced chi square statistic: 0.74 (A) and 0.53 (B).*

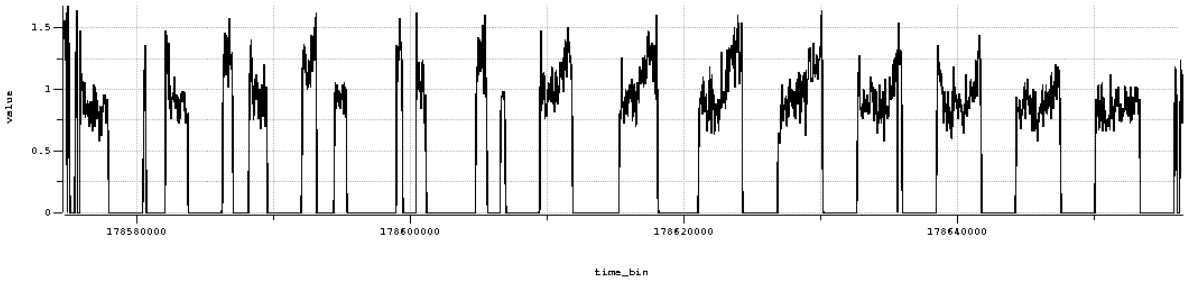

Figure 2.12: *Light curve of module A after adding our own GTI file*

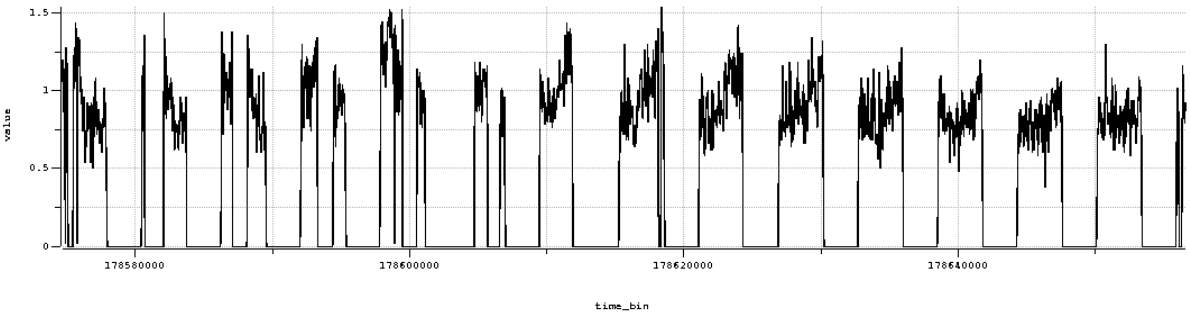

Figure 2.13: *Light curve of module B after adding our own GTI file*

The above light curves look much better than the previous light curves (figure 2.12 and figure 2.13). All extremely high spikes are removed. We also have applied barycenter correction in this step. After adding the GTI file, the cleaned event files are changed too. As a result, the spectra should also have some changes. The figures 2.14 are spectra produced by using GTI files we generated.

The table 2.3 shows some critical parameters of the fitting result. We can see that adding our own defined GTI file will apparently affect the result of spectra fitting. The photon index change from 1.10 to 1.20 for module A while the photon index change from 1.53 to 1.48. Besides, the chi square statistic changes dramatically for both module A and B (nearly doubled). We notice that the column density for module A and B differs greatly. I think we can ignore this for now because hard X-ray is nearly not affected by interstellar medium. We will care about column density after combined with other telescopes data such as Chandra.

Then, we want to combine the module A and B data to fit the spectra together. This leads to a

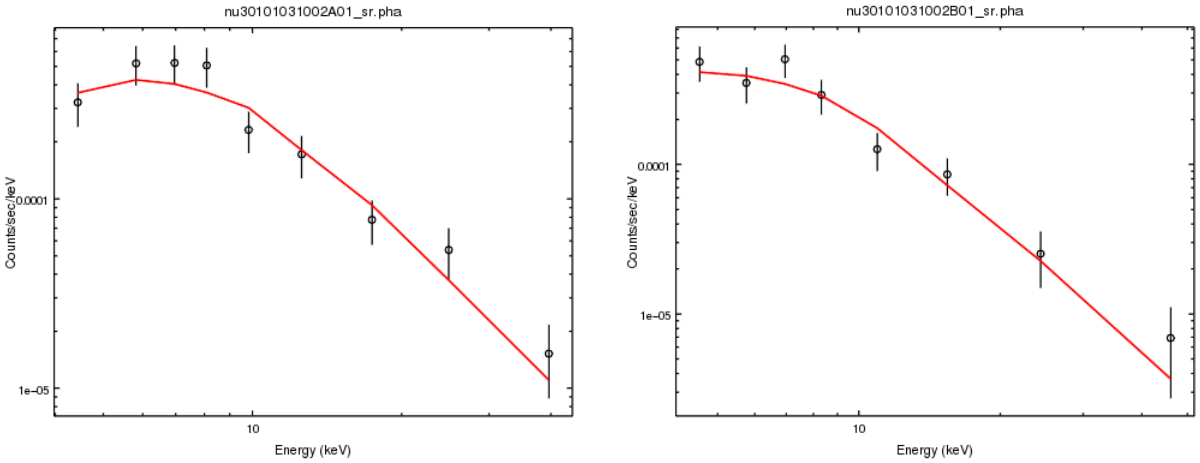

Figure 2.14: *Spectra of module A (left) and B (right) after adding our own GTI files. The total source counts of A before subtracting background is 238 and B is 211. After subtracting background counts, the source counts of A is 177.78 and B is 139.46. Reduced chi square statistic: 1.13 (A) and 0.98 (B).*

	Module A	Module B
Column Density (nH) ($10^{22} atoms/cm^2$)	7.57	4.65×10^{-8}
Photon Index (Γ)	1.20	1.48
Reduced Chi Square Statistic	1.13	0.98

Table 2.3: *Fitting result with user defined GTI files*

question. We know that there are some intrinsic differences between module A and B of *NuSTAR*. As a result, how do we combine two modules together to generate one spectrum? There are two ways of doing this. Firstly, we can directly fit the spectra of these two modules with one single model. Secondly, we can add a constant between module A and B to represent the differences.

Chapter 3

Gamma-Ray Analysis

As mentioned before, because of the very short rotation periods, MSPs have very small light cylinder radii compared with normal pulsars. As a result, their emission mechanisms are similar to normal pulsars, especially for my target objects — PSRJ0218+4232, PSRJ1939+2134 and PSRJ1824-2452 which are among the fastest spinning MSPs. Therefore, as normal pulsars,these three pulsars are bright in Gamma-Ray band so it is convinient for us to analyze the spectra properties of them in gamma-rays.

3.1 Gamma-Ray Emission Mechanism of MSPs

The gamma-ray emissions of MSPs are mainly contributed by curvature radiation so in order to understand the gamma-ray model, curvature radiation should be reviewed first.

3.1.1 Curvature Radiation

This is Curvature Radiation.

3.2 Two-layer Model

After we have reviewed gamma-ray fundmental emission mechanism, we can proceed to the Two-layer model on which this thesis is mainly based.